JOURNAL OF COMPUTATIONAL PHYSICS 66, 391–410 (1986)

β Limits in H-Mode-like Discharges

A. D. TURNBULL, M. A. SECRÉTAN, F. TROYON,
S. SEMENZATO,* AND R. GRUBER

Centre de Recherches en Physique des Plasmas,
Association Euratom - Confédération Suisse,
Ecole Polytechnique Fédérale de Lausanne,
21, av. des Bains-CH-1007 Lausanne, Switzerland

Received December 10, 1985; revised February 12, 1986

DEDICATED TO THE MEMORY OF RAYMOND C. GRIMM

Recent tokamak β optimization studies have indicated the existence of a β limit proportional to the plasma current. A two-step numerical optimization procedure is described for finding β limits in tokamak configurations with peaked current and flat pressure profiles, such as are believed to be characteristic of H-mode plasmas immediately after the L to H transition. Current and pressure-driven instabilities are optimized independently by specifying both the averaged current density and the pressure gradient directly. Direct control over both the global and local characteristics of the pressure profile also permits independent optimization of ballooning modes and the low n kink modes that arise at high β. Results are given for the optimization of a circular cross-section tokamak, computed for one value of the plasma current. An optimized, stable equilibrium is found, with a β that is 50% above the limit predicted for this current.

I. INTRODUCTION

The existence of an operational β-limit in tokamaks appears to be an experimental fact [1–4]. The dependence of this limit on the appropriate parameters conforms to the scaling law for the ideal MHD stability limit found in numerical optimization studies [5–7]. Nevertheless, this agreement still leaves many questions open. For instance, in the optimization studies, β is constrained by the simultaneous requirements of stability to low n kink modes and stability to ballooning modes, whereas in experiments, the limit manifests itself either as a disruption or as confinement degradation. The connection between the theoretical and experimental limits is not yet entirely clear.

"H-mode" auxiliary heated divertor discharges, observed first in ASDEX [8] and

* Permanent address: Control Data Corporation, Zurich, Switzerland.

581/66/2-10

0021-9991/86 $3.00

now also in PDX [9] and Doublet III [10], have been found to recover the ohmic confinement times that are degraded in "L mode" auxiliary heated plasmas. Above a critical density and heating power, a bifurcation of an L-mode discharge is triggered (e.g., by a sawtooth heat pulse), which results in a new H-configuration that is characterized by a broad density profile and a high edge electron temperature and gradient, and consequently by a steep edge pressure gradient [11].

The MHD aspects of the H-mode are only now being explored. One new type of MHD activity that is normally associated with the H-mode, is the regular fluctuations, known as Edge Localized Modes (ELMs) [3, 4, 8, 11–14], that coincide with burst-like releases of particles and energy across the separatrix. The ELMs are generally interpreted as primarily current-driven MHD surface modes [11], possibly caused by a periodic broadening of the current density profile [12]. Another MHD phenomenon, observed so far only in H-mode plasmas, is the deterioration in confinement as the local β is increased in the steep pressure gradient region near the edge. This is attributed to the onset of MHD ballooning modes [13, 14], since it coincides with local violations of the theoretical MHD ballooning limits.

In the context of the β-limit, the experimental results obtained in the H-regime, particularly the most recent ones from the ASDEX group [13, 14] have some intriguing features. When the beam contribution is subtracted, the limiting β in the H-regime appears to be at about the same value as in the L-regime. Yet the transition from the L to H regimes is accompanied by the creation of a very steep temperature gradient at the plasma edge, which, if the current profile followed the electron temperature according to the Spitzer law [15], would imply a steep current gradient at the plasma edge. This would be expected to have adverse effects on MHD stability, and yet the ELM relaxations are the only visible signs of an eventual destabilization. Recent experiments on ASDEX [13, 14] provide evidence that the explanation may be that, at the L to H transition, the fast adjustment of the temperature profile is not accompanied by a discontinuous transition of the current density profile. Instead, the L-mode peaked current density is frozen in after the transition to the H-mode, although it can broaden on a slower transport time scale. Only the pressure profile (along with the density and temperature profiles) becomes very broad at the transition.

There is, so far, no theoretical study of the stability of such profiles. In particular, one consequence of a pressure profile that is much broader than the averaged current density, is the existence of a strong $m = 1$ "Pfirsch–Schlüter" current density in the outer region of the plasma where the pressure gradient is large. There has been no investigation of the effect of currents of this form on MHD stability.

The object of this paper is to present the modifications made to the equilibrium and stability code (EQLAUS/ERATO [16]) to handle profiles of this type, and to present the first stability results obtained from a procedure developed to optimize the β for these profiles. Three types of mode can be distinguished that need to be stabilized in the optimization; instabilities that are driven by the $m = 0$ averaged current density, and two types of "pressure driven" mode. Of these, the low n kink

modes are found to depend only on the global pressure profile (i.e., on β_p) and are a consequence of the $m = 1$ Pfirsch–Schlüter current, whereas the high n ballooning modes are sensitive to the local pressure gradient. We are able to stabilize each type separately by keeping direct and independent control over the averaged current and the global and local features of the pressure profile.

In the following section, we describe the method used to specify the profiles and the class of equilibria chosen for the stability study. The optimization procedure is explained in Section III, and the results of a β-optimization, carried out with this class of equilibria, in a circular cross-section Tokamak of aspect ratio 5, are presented in Section IV. The conclusions from the study are summarized in Section V.

II. Equilibrium

The equilibria used in numerical optimization studies [5, 6, 17–21] are computed by solving the Grad–Shafranov equation for the poloidal flux Ψ,

$$\Delta^* \Psi = -(r^2 p'(\Psi) + TT'(\Psi)). \tag{1}$$

The numerical optimization studies reported to date, have been restricted to a few narrow ranges of equilibrium profiles, either:

(i) $p'(\Psi)$ (pressure gradient) and $TT'(\Psi)$ (toroidal field profile) are specified independently [5, 6, 17, 18] or,

(ii) $p'(\Psi)$ and the safety factor

$$q(\Psi) = T(\Psi)/(2\pi) \int dl/(r|\nabla \Psi|), \tag{2}$$

are specified independently [19–21]. Here, the integral over dl is a line integral over a poloidal cut of the flux surface.

Normally, these are given as functional forms with a few adjustable parameters that can be optimized.

An efficient optimization procedure has two important requirements. First, genuine control over the equilibrium functions is necessary, especially at the endpoints. For example, specifying q provides no control over the edge current density, which is an important determinant of kink stability. On the other hand, when $TT'(\Psi)$ is specified, though the use of polynomial expansions (say 10 terms) provides enough control in principle, in practice, it becomes rather impractical when more than 2 or 3 terms are used to finely tailor the profiles [6].

The second requirement is an "orthogonal" optimization, in which, once one type of mode is stabilized, the parameters are adjusted to stabilize the other modes without modifying the stability of the first mode.

Previous optimization studies have only partially satisfied these two

requirements. Optimization studies of the JET and INTOR devices used polynomial expressions [5, 6] in p' and TT' with only two adjustable terms,

$$p'(\Psi) = \lambda(\Psi + p_2 \Psi^2),$$
$$TT'(\Psi) = \lambda t_1 \Psi.$$

λ is determined from normalization to the total current, and t_1 and p_2 can be varied, keeping ballooning stability marginal for example, until the kink limit is reached. Such a procedure is "orthogonal" but time consuming, and the global polynomial source functions provide limited control. More restricted optimizations for JET have also been carried out using exponential profiles with the same number of parameters [17, 18]. Global representations, however, are not suited to the local adjustments of the gradients that are necessary for optimization [6, 7] against localized stability criteria such as the ballooning criterion.

Other authors [19–21], have suggested the use of q rather than TT', but a search over the (p', q) parameter space is still necessary to find the optimum β. Furthermore, specification of q normally results in a finite current density gradient near the edge, which, as was shown clearly in Ref. [18], can result in surface kinks with small growth rates that cannot always be resolved. At the expense of a significant reduction in β [18, 21], these have been shown to be stabilized by a slight tailoring of the current profile near the edge.

We present an alternative optimization procedure that, whilst avoiding the problem of a finite current density at the plasma surface, retains the advantages of direct control over the q profile. The optimization consists of two steps that are "orthogonal" in the sense that kink and ballooning modes are stabilized independently. Whereas ballooning modes are driven by the local pressure gradient, to a large extent, low n kink modes are driven by either the average current (at low β_p) or the $m = 1$ Pfirsch–Schlüter current (at high β_p) and are insensitive to the details of the pressure profile. We therefore,

(i) specify $p'(\Psi)$, and either $I'(\Psi)$, the derivative of the current contained within a given flux surface,

$$I'(\Psi) \equiv \int j_\phi \, dl/(|\nabla \Psi|), \tag{3a}$$

or equivalently the poloidal average of j_ϕ,

$$J(\Psi) \equiv \int j_\phi \, dl/(|\nabla \Psi|) \Big/ \int dl/(|\nabla \Psi|), \tag{3b}$$

and,

(ii) construct these profiles from simple piecewise polynomials, matched to keep them differentiably continuous.

The first feature provides us with the desired direct control over the driving forces of the most important instabilities. The second feature provides independent local control over the profiles, enabling, for example, the ballooning modes to be stabilized by local adjustments of the pressure gradient once the global features have been optimized for the low n kink modes. A third feature of our approach is to begin with the zero β case. We find the stability criteria at zero β, and, for the optimization at finite β, we use those criteria to define an operating regime in which the modes that are driven by the average $m = 0$ current are stable.

The above procedure has two further advantages:

(i) One can compute a series of equilibria with increasing β_p but, as far as is possible, with the same magnetic geometry.

(ii) It offers the possibility of directly specifying H-mode profiles in which the pressure profile is much broader than the current profile. The stability results can then be related to the MHD activity that is observed experimentally in H-mode discharges.

Given $p'(\Psi)$ and $I'(\Psi)$, then $TT'(\Psi)$ is computed from

$$TT'(\Psi) = -\left(I'(\Psi) + p'(\Psi)\int r\, dl/|\nabla\Psi|\right)\Big/\int\frac{dl}{(r|\nabla\Psi|)}. \tag{4}$$

To remain the minimum flexibility necessary for adjusting the profiles independently in the centre and edge regions, at least three polynomial sections are required for each profile. Furthermore, to ensure that the mapping from Cartesian (r, z) coordinates to the flux surfaces is accurately represented, the profiles and at least their first derivatives must be continuous. This can be guaranteed by taking third order polynomials in each section. The complete specification of the profiles would then require a total of ten parameters for each profile; the coordinates of the interior nodal points, and the value and derivatives at each node, including the endpoints.

To reduce the number of free parameters to a more manageable level, for most purposes, we can impose the conditions that $I'(\Psi)$ and $p'(\Psi)$ be linear in the outermost and innermost regions, respectively, thus removing four parameters. This only affects the higher order behaviour of the profiles in the respective regions, and is relatively unimportant for stability. Note that similar conditions could not be imposed in the central sections without sacrificing the continuity conditions, nor in the other two end sections without sacrificing the flexibility to treat a variety of configurations. Nevertheless, one more parameter can still be removed, with only a small loss of generality, by requiring that $p'(\Psi)$ be stationary at the node between the last two sections. This restriction allows us to simulate the H-mode pressure profile by setting the peak pressure gradient near the surface.

Taking $s \equiv (\Psi - \Psi_0)/(\Psi_s - \Psi_0)$, where Ψ_0 and Ψ_s represent the values at the axis and plasma surface, respectively, then in the most general case that we therefore need consider, we prescribe (see Fig. 1),

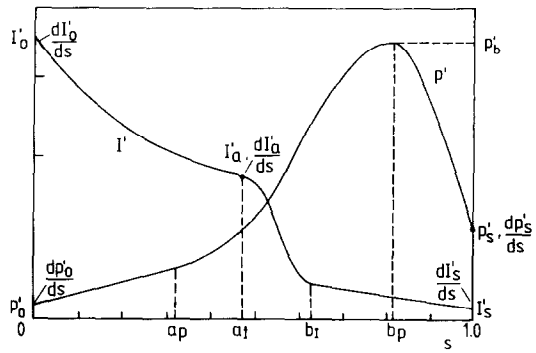

FIG. 1. Current $I'(\Psi)$ (or $J(\Psi)$) and pressure gradient $p'(\Psi)$ profiles versus $s=(\Psi-\Psi_0)/(\Psi_s-\Psi_0)$. The profiles are defined in three separate sections delineated by $s=a_I, b_I$ and $s=a_p, b_p$, respectively. a_I, b_I, a_p, and b_p are specified, as well as the values and derivatives of I' and p' that are shown at $s=0, a, b$, and 1. For clarity, the sign of p' is reversed in the diagram.

$$I'(\Psi)=\begin{cases} a_1+b_1s+c_1s^2+d_1s^3, & 0<s<a_I \\ a_2+b_2s+c_2s^2+d_2s^3, & a_I<s<b_I \\ a_3+b_3s, & b_I<s<1 \end{cases} \tag{5a}$$

and

$$p'(\Psi)=\begin{cases} e_1+f_1s, & 0<s<a_p \\ e_2+f_2s+g_2s^2+h_2s^3, & a_p<s<b_p \\ e_3+f_3s+g_3s^2+h_3s^3, & b_p<s<1. \end{cases} \tag{5b}$$

The coefficients for $I'(\Psi)$ are directly determined from the values of $I'(\Psi)$ and its derivative at $s=0$ (I'_0 and dI'_0/ds), at $s=1$ (I'_s and dI'_s/ds), and at $s=a_I$ (I'_a and dI'_a/ds). For $p'(\Psi)$, we determine the coefficients from the values and derivatives of $p'(\Psi)$ at $s=0$ and $s=1$ (p'_0, dp'_0/ds, p'_s and dp'_s/ds), and from the value at b_p (p'_b) where $p'(\Psi)$ is assumed to be at its maximum. The remaining coefficients are defined by the eight conditions for continuity of $I'(\Psi)$ and $p'(\Psi)$ and their first derivatives.

This prescription provides enough flexibility to obtain reasonable safety factor profiles in the wide variety of configurations that we have so far considered. In normal operation, p'_0, dp'_0/ds, I'_s, and dI'_s/ds are set to zero so that there is no pressure gradient at or near the axis, and the current density and its gradient vanish at the edge of the current channel. This ensures that the Mercier Criterion is satisfied in the vicinity of the axis, and avoids the current-driven surface modes that are associated with finite edge current density. For the remaining free parameters governing $I'(\Psi)$, I'_0 determines the total current (or q_s; the value of q at the surface), I'_a, dI'_0/ds, and dI'_a/ds determine the shape of the q profile, a_I defines the width

of the current channel (or q_s/q_0; the global shear), and b_I defines the steepness of the current drop.

For the examples with circular cross-section that we consider here, we can reduce the number of free parameters still further by confining ourselves to the simplest possible situation. In that case, it is sufficient to take a rounded Shafranov current density profile [22] by setting dI'_0/ds and dI'_a/ds equal to zero, and taking $I'_a = I'_0$, thus fixing the shape of the q profile, and by fixing $b_I - a_I$; this parameter having little effect on ideal MHD stability, although it does affect the numerical resolution. Then at zero β, this defines a two-dimensional operating space, over which, the kink stability boundaries can be determined (by varying b_I) at any total current (i.e., given I'_0). The q-profiles that we obtain in a circular cross-section equilibrium, using the Shafranov current density profile, are almost always flat over a large region in the centre, with high shear only near the edge.

For the parameters that define $p'(\Psi)$, p'_b is determined by the required β_p, and the two parameters a_p and b_p are determined by the requirements for ballooning stability. We still have the possibility of allowing a finite pressure gradient and zero average current density right at the surface. It is not clear what effect the resulting oppositely directed Pfirsch–Schlüter *surface* currents will have. For our purposes, we take the simplest possible case by neglecting this possibility and setting $p'_s = 0$, but we keep the pressure gradient large as near to the surface as numerical resolution allows. The influence of finite edge pressure gradient is deferred to a later study. For the purpose of illustrating the optimization procedure, one final parameter can also be fixed by imposing a condition on the derivative of $p'(\Psi)$ at the surface. This is most easily achieved by requiring that $p'(s)$ be quadratic in the last section. This is, of course, a purely arbitrary restriction, but it serves the purpose of limiting the number of free parameters to a manageable number, whilst minimizing spurious higher order variations of the profile.

We now briefly mention the numerical aspects involved in converting the standard equilibrium code (EQLAUS), with p' and TT' given as polynomials, to the new code in which p' and I' are given. The equilibrium is computed using an (r, z) Grad–Shafranov code that assumes a fixed boundary, with the total toroidal current given. Symmetry in the $z = 0$ plane is assumed. On each iteration, we require the integrals $\int r\, dl/|\nabla\Psi|$ and $\int dl/(r|\nabla\Psi|)$. The N_p flux surfaces are mapped from the magnetic axis out along N_t angular rays by interpolation from the (r, z) grid flux values. This defines $\rho(\Psi, \Theta)$ and $\nabla\Psi$, where ρ is the radius vector from the magnetic axis. The integations are then calculated by quadratures. $TT'(\Psi)$ is computed using Eq. (4), at the (r, z) mesh points, from quadratic interpolation of the integrals known on the (Ψ, Θ) mesh. Accuracy is kept as close as possible to second order in the equilibrium mesh. Normally, best convergence and accuracy for circular cross-section equilibria is obtained with $N_p \sim N_t \sim N_r/3 \sim 2N_z/3$.

Convergence is generally about a factor three slower with $I'(\Psi)$ than with the standard code, and total computation time increases by roughly a factor 10. For noncircular cross-sections, convergence is even slower. However, this drawback can be alleviated by using $J(\Psi)$ (Eq. (3b)) rather than $I'(\Psi)$. One extra surface integral

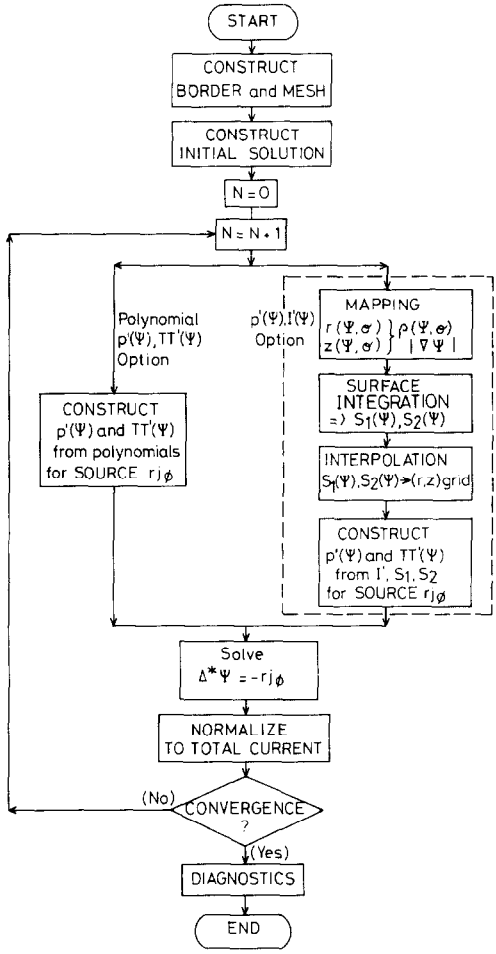

FIG. 2. Flow diagram for the modified EQLAUS equilibrium code. The modifications for specifying $I'(\Psi)$ or $J(\Psi)$ are enclosed by the box (— — —).

is required, but the convergence rate improves dramatically, and is faster than the standard code in most cases of interest, especially at high resolution. With $J(\Psi)$, the time required to calculate a high resolution equilibrium ($N_r \times N_z \simeq 240 \times 120$), is generally a factor two to three greater than for the standard code (EQLAUS), the extra time being consumed almost entirely in the mapping of the flux surfaces required at each iteration.

An outline of the equilibrium code is shown in Fig. 2. Stability is computed from the variational finite hybrid-element code ERATO [16]. For this purpose, $p'(\Psi)$ and $TT'(\Psi)$ are fed in from the equilibrium code as tables, and interpolated in ERATO, onto the ERATO grid.

III. Optimization Procedure

In the one-dimensional cylindrical limit, it is possible to find arbitrarily high β, stable equilibria by taking a flat current profile with a current-free region, of some critical width, near the surface (i.e., a hard core pinch), and by placing all of the pressure gradient within the current-free region [22] . In a torus, such a configuration is limited by high β pressure-driven modes; ballooning modes and the so-called "ballooning-type" kink modes [23]. In a torus, the current-free region can only be current free on average over a flux surface. Current-driven instabilities can still arise at finite β from the presence of Pfirsch–Schlüter currents, and these could also limit the achievable β, However, one can still expect that the kink limit would remain high and that the ballooning limit could be increased by spreading the pressure gradient inside, until it is marginally stable, without affecting the kink stability.

Therefore, by taking the simplest possible case, namely the rounded Shafranov current profile that was proposed in the previous section, we can optimize against kink stability at a given total current with the aid of just one other parameter, and, by using the pressure gradient profile that was also proposed in Section II, we can hope to obtain reasonably high β equilibria with profiles that mock the main features of the H-mode. To illustrate the optimization procedure, we will therefore confine ourselves to this simplified situation. Nevertheless, it should be kept in mind that the procedure can be generalized to include further optimization over the other parameters, for example, over the shape of the q profile, or by allowing finite pressure gradients right at the edge.

Our optimization requires a knowledge of the stability properties of a given configuration at zero β, so that we can optimize the β from a sound basis. The results of a general parameter survey at zero β are described elsewhere [24], but for our circular cross-section, with the profiles described in Section II, the results can be summarized as follows: Stability against $n=1$, $m=2$ surface kinks requires that $q_s > 2$. Stability against free-boundary "toroidal kinks" [24] requires $q_0 > 1$. In addition, $q_s > \alpha(q_0)\, q_0$ is required to avoid higher (n, m) surface kink modes [18, 24], where $\alpha \simeq 1$ for the rounded Shafranov profiles that we are using. At finite β, we assume that these criteria are still necessary (though not necessarily sufficient) for stability against purely current-driven modes. This assumption simplifies the optimization procedure by restricting the parameter range, during the later β optimization steps, to avoid the region in which the kinks driven by the average current-density are already unstable. Costly convergence studies on the small growth rate modes that can arise when $q_0 < 1$ or $q_s < \alpha(q_0)\, q_0$ are thereby avoided. The assumption has been validated by the finite β stability results obtained so far, in which convergence studies always predict instability when the criteria are violated.

The optimization proceeds in two main steps. For fixed constant current, the β is maximized with regard to kink stability by varying the current channel width b_f. An equilibrium is considered stable for this purpose, if it satisfies a σ^2 criterion [25]

of $\sim 10^{-4}$, and it satisfies the zero β stability criteria mentioned above. During this step the pressure gradient is maintained outside the current channel (i.e., $a_p = b_I$), and the resulting equilibrium is normally strongly ballooning unstable. As well as taking advantage of the area weighted definitions of β and β_p, keeping p' in the current-free region spatially separates the two principal instability driving terms. In particular, the $m = 0$ and $m = 1$ parts of the current profile are spatially decoupled.

The second step stabilizes the ballooning by spreading the pressure gradient inside at constant β_p. This has a relatively small effect on the kink stability since the average current density is maintained constant and the equilibria are therefore affected as little as is possible. Only small adjustments are then required to obtain the optimum. The kink is generally destabilized slightly, since spreading the pressure inside at fixed current tends to decrease q_0, and this can drop below unity. In addition, there can be some residual ballooning instability once the pressure gradient is spread all the way to the axis. The former is stabilized by a small adjustment in the current channel width at constant β_p. The latter can be stabilized either by a small adjustment in the position of b_p, by optimizing over dp'_s/ds, or by a small drop in β_p. The final β should not be lowered much from the original kink stable equilibrium that was obtained after the first step.

The intermediate n ideal modes (n = toroidal mode number) are ignored during the optimization; these are assumed to be stable if the $n = 1$ and infinite n ballooning modes are stable. Their stability can always be checked after the optimization is completed. On the other hand, the constraints imposed by tearing modes in the steep current gradient region may be important, and these have also been ignored in the present work. If necessary, tearing modes could probably be stabilized by a further rounding of the current profile, since the steepness of the drop is a free parameter.

The important feature of the optimization is that the kink and ballooning stability are strongly affected by the widths of the current and pressure profiles respectively but are only weakly affected by the converse. Furthermore, to the extent that the kink modes can be driven unstable at high β, they are essentially only affected by the global β value, whereas the ballooning stability is dependent on the local pressure gradient. In the optimization described here, these parameters are directly and independently controlled.

IV. Results and Discussion

We consider, as an example, a circular cross-section equilibrium with aspect ratio $R/a = A = 5$. Four series of equilibria with increasing poloidal β were constructed at constant normalized current, $I_N = \mu_0 I/R_0 B_0$, by varying the channel width b_I, and the stability of each was determined for the $n = 1$ free-boundary kink mode using the ERATO stability code. We use an equilibrium mesh $N_r \times N_z$ of 160×80, $N_p \times N_t$ is set at 40×40, and the equilibria are iterated to a maximum residue in Ψ

of 10^{-6}. For these cases, we specified $I'(\Psi)$. Stability was determined using a mesh of 80 flux surfaces and 40 poloidal angles χ.

The results are displayed in Fig. 3. The equilibria that are stable at higher β_p correspond to those with the current channel further inside. The pressure gradient was kept outside the current channel in each case. The four series labelled E, F, G, and H are defined by: $b_I = 0.75$, 0.70, 0.65, and 0.60 respectively. $b_I - a_I$ is fixed at 0.20, $a_p = b_I$, and $b_p - a_p = 0.15$. The values of q_0 and q_s are shown for the calculated points. The ballooning limits for each case are also indicated on the horizontal axis. For the H-mode profiles that we are considering, we find that ballooning is a much more stringent criterion than kink stability.

The unstable equilibria for $q_0 > 1$, $q_s > 2$ can be classified into two types. In either case, the modes may be interpreted as either "pressure-driven" or "current-driven," since the pressure gradient is always associated with a Pfirsch–Schlüter current.

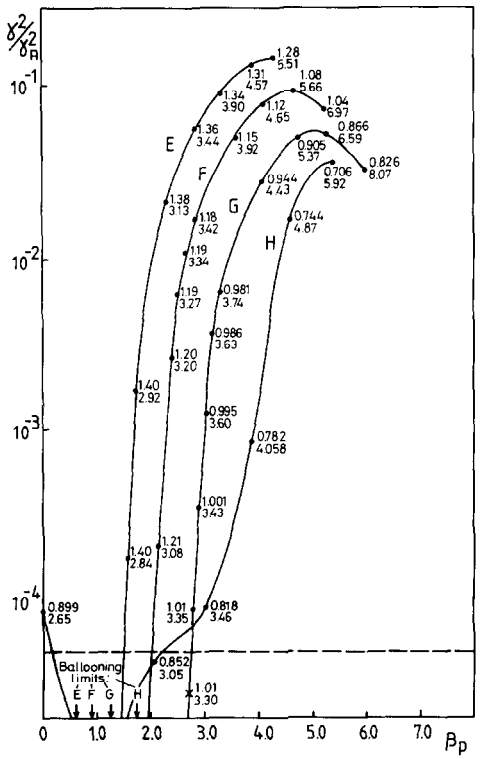

FIG. 3. Growth rates versus β_p for the four series (E, F, G, and H) of circular cross-section equilibria. The growth rates are normalized to an Alfvén transit frequency γ_A. Each series corresponds to a sequence of equilibria at increasing β_p with the same average current profile ($I'(\Psi)$). The four series correspond to current profiles of decreasing width defined by $b_I = 0.75(E)$, $0.70(F)$, $0.65(G)$, and $0.60(H)$. In all cases, $b_I - a_I = 0.20$, $a_p = b_I$, and $b_p - a_p = 0.15$. The values of q_0 and q_s are indicated for each of the computed equilibria, and the ballooning limits for each series are shown. The optimum kink-stable equilibrium for a σ^2 criterion of 0.5×10^{-4} is indicated by an "$\times$."

When the current channel is narrow or β is high enough, the instabilities are free-boundary modes, analogous to the internal "ballooning-type" kinks discussed in Ref. [23], and are normally categorized as pressure-driven modes. Examples are shown in Figs. 4a and b. Fig. 4a corresponds to a case in the F-series with $q_0 = 1.153$, $q_s = 3.923$, and $\beta_p = 3.513$. The instability is strongly ballooning on the outside of the torus and has a relatively large growth rate. Inside the $q = 2$ surface, the mode is an $m = 2$ kink, coupled to predominantly $m = 3, 4$ components within the other q surfaces, and to an $m = 5$ component right near the edge. As the mode becomes more marginal, (Fig. 4b), it becomes more localized and a more complicated structure emerges, but the evidence of a ballooning component is still apparent. This mode corresponds to one of the G-series with $q_0 = 1.0006$, $q_s = 3.4345$, and $\beta_p = 2.904$. The poloidal mode structure is the same as in Fig. 4a, but in this case, there is a strong radial modulation in amplitude.

When the current channel extends further out, the mode structure is modified, as in Fig. 4c, and the mode resembles a current-driven surface kink [18, 24]. This case

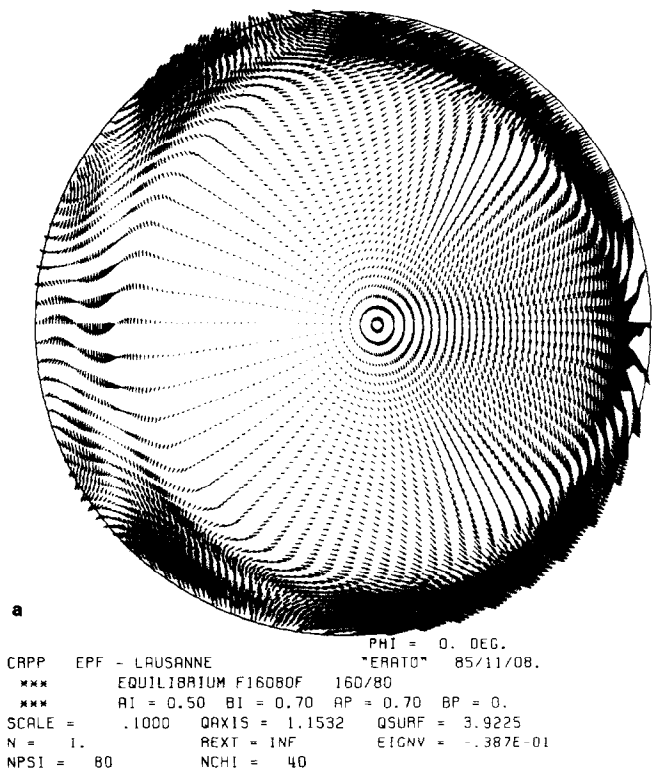

FIG. 4. Mode structures of free-boundary finite-β kinks. (a) Unstable high β, $q_0 = 1.153$, $q_s = 3.923$, $\beta_p = 3.513$, and $\gamma^2/\gamma_A^2 = 0.0387$. (b) Weakly unstable, narrow current; $q_0 = 1.0006$, $q_s = 3.434$, $\beta_p = 2.904$, and $\gamma^2/\gamma_A^2 = 0.000261$. (c) Weakly unstable, broad current; $q_0 = 1.404$, $q_s = 2.841$, $\beta_p = 1.450$, and $\gamma^2/\gamma_A^2 = 0.000182$.

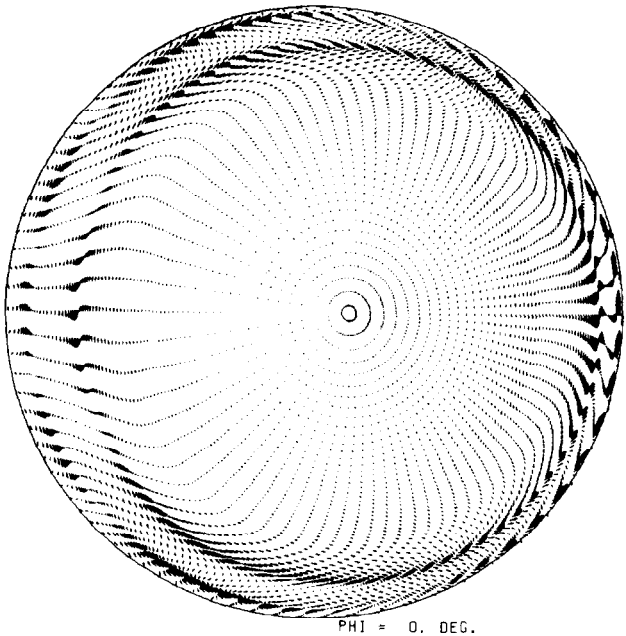

b

PHI = 0. DEG.

CRPP EPF - LAUSANNE "ERATO" 85/11/06.
*** EQUILIBRIUM G16080M 160/80
*** AI = 0.45 BI = 0.65 AP = 0.65 BP = 0.
SCALE = .1000 QAXIS = 1.0006 QSURF = 3.4345
N = 1. REXT = INF EIGNV = -.261E-03
NPSI = 80 NCHI = 40

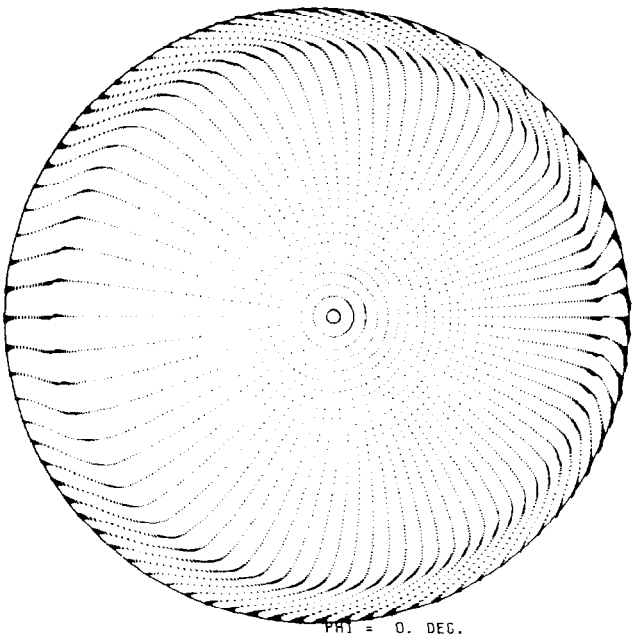

c

PHI = 0. DEG.

CRPP EPF - LAUSANNE "ERATO" 85/11/06.
*** EQUILIBRIUM E16080P 160/80
*** AI = 0.55 BI = 0.75 AP = 0.75 BP = 0.
SCALE = .1000 QAXIS = 1.4043 QSURF = 2.8409
N = 1. REXT = INF EIGNV = -.182E-03
NPSI = 80 NCHI = 40

FIG. 4—*Continued.*

has $q_0 = 1.404$, $q_s = 2.841$, and $\beta_p = 1.450$, and would be stable according to the zero β criteria for current-driven modes since $q_s > \alpha(q_0)\, q_0$. One can conclude that the zero β current-driven surface mode is destabilized by the finite pressure gradient if the current channel is too broad. The higher n modes are even more unstable than the $n = 1$ mode shown here, and, although the ballooning component is more prominent, they still have the same general features; they are highly localized near the edge, and they have the appearance of current-driven modes that are destabilized only at finite β by the Pfirsch–Schlüter current. These modes (most likely the higher n Fourier components) could therefore be responsible for the ELM's that are observed experimentally in H-mode discharges [3, 4, 8, 11–14]. The onset of the instability seems to require a sufficiently high β and a sufficiently broad current profile. This is consistent with the results reported in Refs. [12–14]. As the plasma evolves on a transport time scale, the averaged current profile, which was frozen in from the L-mode transition, broadens until it triggers the ELM, after which, the plasma relaxes to a more stable configuration by restricting the current and increasing the shear. The sequence is repeated in a sawtooth-like fashion [11–14]. One can picture the plasma as evolving and relaxing, at essentially constant β_p, through the series E, F, G, and H in Fig. 3. According to this scenario, in ELM-free discharges [3], the artificially enhanced radiation could modify the transport [14], in such a way as to limit the broadening of the current profile, thereby suppressing the ELMs.

To optimize the β, we choose the highest β_p equilibrium that is stable according to a σ^2 criterion of 0.5×10^{-4} and the zero β criteria for current-driven modes discussed earlier. The toroidal kinks that are destabilized when $q_0 < 1$, have growth rates that scale with $(a/R)^k$ over the standard kink mode ordening, where $k \sim 2q_s$. They cannot therefore always be resolved by the σ^2 criterion that we have chosen. The zero β criteria imply that the entire curve labelled H is rejected since $q_0 < 1$. Nevertheless, in this particular case, the chosen kink-optimized equilibrium, indicated by an "$\times$" in Fig. 3, coincides with the highest β, stable equilibrium as determined by the σ^2 criterion alone, indicating that our choice of σ^2 is a reasonable one in the sense that it does resolve the slowly growing toroidal kinks. However, at lower currents where q_s is larger, the growth rates for these modes would not have been resolved by the σ^2 criterion alone. We have also verified the σ^2 criterion for this particular case by convergence studies, which showed that the chosen equilibrium is, in fact, stable, but that the point above on the same curve ($q_0 = 1.006$, $q_s = 3.346$) is unstable.

The kink-optimized equilibrium is strongly ballooning unstable. Spreading $p'(\Psi)$ inside ($a_p \to 0$) at constant β_p stabilizes most of this but slightly destabilizes the kink in two ways; q_0 drops below unity and the pressure-driven ballooning-type kink is marginally destabilized. Decreasing β_p would stabilize both of these and the residual ballooning, but does not give the optimum β. On the other hand, moving b_p, either further destabilizes the kink or the ballooning. Instead, however, by moving the current channel outwards slightly at constant β_p, q_0 is raised to stabilize the current driven mode. The pressure driven mode is stabilized at the same time if b_p is

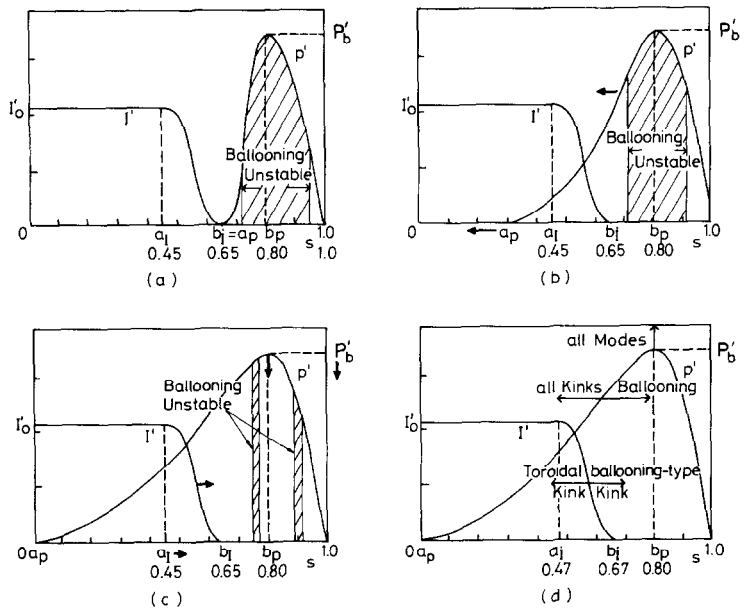

FIG. 5. Sequence of profiles at various stages of optimization. (a) Kink-optimized equilibrium profiles. The ballooning-unstable region is indicated. (b) Ballooning stabilized by spreading the pressure gradient inside at constant β_p. (c) Pressure gradient spread until $a_p = 0$. Some residual ballooning-unstable surfaces remain and the toroidal kink ($q_0 < 1$) and ballooning-type kink are slightly destabilized. (d) Final optimum β equilibrium stabilized by a small shift in the current profile and a small drop in β_p. Further changes in the profiles, except decreasing β_p, result in the destabilization of the various modes shown.

held fixed, leaving only the residual ballooning region unstable. This is then stabilized by a relatively small drop in β_p, from 2.63 to 2.47, keeping all else fixed, The final β is only about 10% lower than the kink-optimized equilibrium with all the pressure gradient outside the current channel.

The complete optimization sequence is illustrated in Fig. 5. The q profiles for the original kink-optimized equilibrium and the final fully optimized stable equilibrium are shown in Fig. 6. These are plotted against the ERATO coordinate $s_E = \sqrt{s}$ [16]. The strong edge shear stabilizes the plasma against the large pressure gradient near the surface. The q profiles are also extremely flat in the centre, ensuring that q_0 remains above unity, despite the strong edge shear. Also shown are the profiles of the source function $TT'(s)$. The important feature here is the change in sign near the outer edge. There, TT' is of opposite sign to the pressure gradient so that the nett toroidal current vanishes on average over a flux surface.

The optimized equilibrium has been checked for stability against higher n modes ($n = 1, 2, 3$ and 4) and convergence checked for instability with σ^2 less than 10^{-6}. The final, stable, optimum β equilibrium has $a_I = 0.47$, $b_I = 0.67$, $a_p = 0.0$, $b_p = 0.80$, and has $\beta_p = 2.47$ with $\beta = 1.58\%$. This is to be compared with the limiting value

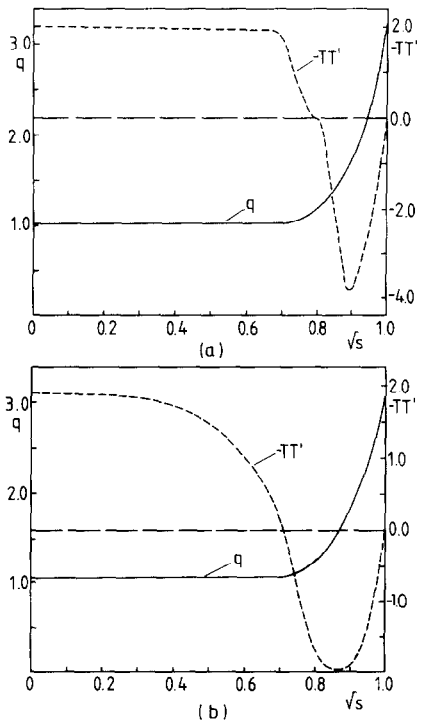

FIG. 6. Safety factor $q(\Psi)$ and Toroidal Field Function $TT'(\Psi)$ versus the ERATO coordinate $\sqrt{s}$ for (a) kink-optimized and (b) fully optimized equilibria.

[5] of $\beta_T = 2.2 I_N A$, where $I_N = \mu_0 IA/R_0 B_0$ is the normalized current. For our case, $I_N = 0.10$ and $\beta_T = 1.1\%$.

With the optimization procedure that we have used, and the profiles we have chosen, we are therefore able to raise the kink limitation in the scaling of Ref. [5], and find equilibria that are limited predominantly by ballooning. In fact, the β is about 10% above the ballooning limit of $\beta_W = 2.8 I_N A = 1.4\%$, found by Wesson and Sykes [7] for circular cross-section equilibria in the large aspect ratio limit. The optimized current and safety factor profiles obtained here, are also quite similar to those obtained in Ref. [7]. However, in our case, the pressure profile has not been completely optimized against ballooning; this would require that $p'(\Psi)$ be marginal everywhere. In principle, this could be done if the pressure profile is defined piecewise using a large enough number of nodes. The β could then be raised well above the Wesson–Sykes limit.

Even with the simplifying restrictions that we have imposed, further optimization of the pressure profile is possible since the parameters b_p, p'_s, and dp'_s/ds (as well as p'_0 and dp'_0/ds if the Mercier Criterion is not too restrictive) are still at our disposal. A more complete optimization could be made, for example, by optimizing for the ballooning by varying both a_p and b_p simultaneously. The kink might be

destabilized by a greater amount in that case, but could still be restabilized by a shift in the current profile. Alternatively, one could try to remove the residual ballooning by varying dp'_s/ds, but this could not stabilize the small ballooning unstable region inside the node b_p, so b_p and dp'_s/ds would also have to be optimized simultaneously. The introduction of another parameter, however, would make the optimization unmanageable, and would not necessarily lead to the steep edge pressure gradient of the *H*-mode configuration, consequently, we have not attempted further optimization. The equilibrium that we have obtained is marginally ballooning stable only in the steep pressure gradient region near the edge. This is consistent with the recent results reported in Ref. [14].

The experimentally observed *H*-mode equilibria generally lie close to or below the limit β_T. The improvement over this value is presumably a result of the Shafranov profiles that we have assumed. These are known to be more optimistic for purely current-driven modes, both in a straight cylinder [22], and in toroidal geometry [24]. Furthermore, they are quite similar to the profiles obtained in Ref. [7] for the optimum-β ballooning-stable equilibrium, in the large aspect ratio limit of a circular cross-section tokamak. More realistic *H*-mode profiles, in which the averaged current density is not strictly zero in the outer region, would probably result in a lower β limit for the low n kink modes. Nevertheless, the same physical processes as discussed here, would still be expected to operate. The Shafranov profiles could possibly even be realized experimentally if current-drive were employed to tailor the current density profile independently of the pressure gradient. The results of the present study would then predict a significant improvement in β.

The high β that we have obtained in this particular case may still be fortuitous, however, since q_s is just above three, and there is some evidence [5,21] that the limit in Ref. [5] has some modulation, with peaks just above the integer q_s values. Nevertheless, such a strong modulation for circular cross-section equilibria would be unprecedented.

To conclude this section, we now consider an interesting feature of Fig. 3. As β_p is increased for fixed current, the equilibrium becomes more unstable as expected. There are three competing effects operating. Increasing β_p increases the free-energy available for pressure-driven modes, but also decreases q_0, even though q_s increases. The change in q_0 is minimal, but the increase in shear, which tends to be stabilizing, is significant. Also, increasing the width of the current-free sheath, tends to increase the β_p at which instability sets in. q_0 is decreased substantially as this is done, but again the stabilizing shear increases.

We therefore have two separate ways of increasing the shear, either by increasing the pressure gradient maximum, or by decreasing the current channel width. In both cases, increasing shear is associated with increasing β_p, but the latter is stabilizing, and, at low β, the former is destabilizing for the kink. This and the fact that the growth rates for each curve do, in fact, show a stabilizing trend at high β_p, suggests the possible existence of a second stability region for free-boundary kink modes, analogous to the second stability regions for ballooning modes [26] and

the internal kink [27]. At present, numerical convergence problems prevent an extension of the curves, so the existence of the second stability region remains undecided.

V. Conclusions

From the results of Ref. [7] and this study, it seems that there is probably a unique, stable, optimum-β equilibrium, in which the current profile is determined by low n kink stability, and the pressure gradient is determined by large n ballooning stability. A well-defined optimization procecure can be constructed for finding this equilibrium, in which the profiles are defined in terms of splines, with the nodal values of the pressure profile uniquely optimized against the ballooning criterion, and the current profile similarly optimized against kink stability. Such a procedure could possibly be formulated variationally.

The simplified algorithm described in this work, preserves the most important features of the general procedure, namely prescription of the profiles locally in terms of the nodal values, and independent control over the two major driving forces behind the instabilities, i.e., over the current and pressure profiles, so that kink and ballooning stability can be optimized independently. The simplification consists of the reduction in the number of nodal values that are prescribed, yet the most important gross features of the profiles, width, steepness, etc., are still prescribed directly.

The results from an optimization study of circular cross-section equilibria, with profiles modelled on those of H-mode discharges, can be summarized as follows:

(i) For the type of profiles that we have taken, the ballooning limit is generally much more severe than the external kink limit. The intermediate n modes lie between these two limits. This result is surprising in that it is in contrast to the usual situation in previous studies [5, 6, 17–21].

(ii) Despite the reversal in the kink and ballooning limits, we find that the optimum occurs when the ballooning and low n kink limits roughly coincide. This seems to be true in all previous optimization studies, indicating that the two types of mode are driven by physical mechanisms with opposing tendencies. Yet the two types of mode are driven by different physical mechanisms; the low n kinks depend on global features of the current and pressure profiles, whereas the ballooning modes depend on local details of the pressure gradient. In this sense, the β limits for kink and ballooning modes are mutually independent. This is clear from the fact that an optimistic choice of current profile such as ours, can raise the low n kink limit well above the limit in Ref. [5], and that by optimizing the pressure profile, the high and intermediate n mode limits can also be raised to this value.

(iii) We have found H-mode like, circular cross-section equilibria, stable to both ballooning modes and to ideal $n \leqslant 4$ kink modes at $\beta_p = 2.47$ and $\beta = 1.58\%$.

This is 50% above the limit given in Ref. [5], and 10% above the limit given in Ref. [7] for this current.

(iv) The Wesson–Sykes ballooning limit [7] can probably also be surpassed by more than the few percent achieved here, if a finite pressure gradient is admitted at the surface, or if a complete ballooning optimization is performed over the whole pressure profile.

(v) We have identified a mode that may be responsible for the ELMs that are observed in H-mode plasmas [3, 4, 8, 11–14]. The mode has the features of a current-driven MHD surface mode, but requires a sufficiently high β, as well as a sufficiently broad current channel.

(vi) We have found evidence for the possible existence of a second region of stability for external free-boundary kink modes.

The algorithm described here, though applied only to circular cross-section, is applicable to noncircular cross-sections such as bean or racetrack shapes, where specification of TT' in the usual way generally results in either extremely high shear equilibria or hollow q profiles.

ACKNOWLEDGMENTS

The authors have benefitted greatly from numerous discussions with colleagues A. Roy and O. Sauter. This work was partly supported by the Swiss National Science Foundation.

REFERENCES

1. F. TROYON AND R. GRUBER, *Phys. Lett. A* **110**, 29 (1985).
2. G. H. NEILSON, A. J. WOOTTON, J. D. BELL, C. E. BUSH, A. CARNEVALI, *et al.*, *Nucl. Fusion* **25**, 825 (1985).
3. M. KEILHACKER, G. FUSSMANN, G. VON GIERKE, G. JANESCHITZ, M. KORNHERR, *et al.*, "Plasma Physics and Contr. Nucl. Fusion Research," *Proceedings of the 10th Int. Conference, IAEA, London 1984* (Vienna 1985), Vol. 1, p. 71.
4. K. M. MCGUIRE, in *Proceedings of the 1984 Int. Conf. on Plasma Physics, Lausanne, Switzerland, 1984*, Vol. 1, p. 123.
5. F. TROYON, R. GRUBER, H. SAURENMANN, S. SEMENZATO AND S. SUCCI, *Plasma Physics, and Contr. Fusion* **26**, 209 (1984).
6. F. TROYON, R. GRUBER, AND H. SAURENMANN, NET Report, EUR XII – 324/14, Brussels (unpublished).
7. J. A. WESSON AND A. SYKES, *Nucl. Fusion* **25**, 8 (1984); A. SYKES, M. .F. TURNER, AND S. PATEL, "Contr. Fusion and Plasma Physics," *Proceedings of the 11th Europ. Conf., Aachen, F.R.G., 1983*, Part II, p. 363.
8. F. WAGNER, G. BECKER, K. BEHRINGER, D. CAMPBELL, A. EBERHAGEN, *et al.*, *Phys. Rev. Lett.* **49**, 1408 (1982).
9. S. M. KAYE, M. BELL, K. BOLL, D. BOYD, K. BRAU, *et al.*, "Contr. Fusion and Plasma Physics," *Proceedings of the 11th Europ. Conf., Aachen, F.R.G.*, 1983, Part I, p. 19.
10. K. H. BURREL, "Contr. Fusion and Plasma Phys.," *Proceedings of the 11th Europ. Conf., Aachen, F.R.G., 1983*, Part I, p. 11.

11. M. KEILHACKER, G. BECKER, K. BERNHARDI, A. EBERHAGEN, M. ELSHAER, *et al.*, *Plasma Phys. and Contr. Fusion* **26**, 49 (1984).
12. O. GRUBER, in *Proceedings of the 1984 Int. Conf. on Plasma Physics, Lausanne, Switzerland 1984*, Vol. I, p. 67.
13. M. KEILHACKER, G. VON GIERKE, E. R. MILLER, H. MURMANN, F. SOLDNER, *et al.*, *Plasma Phys. and Contr. Fusion* **28**, 29 (1986); M. KEILHACKER *et al.*, *Nucl. Fusion* **25**, 1045 (1985).
14. G. VON GIERKE, M. KEILHACKER, R. BARTIROMO, G. BECKER, H. S. BOSCH, *et al.*, "Contr. Fusion and Plasma Phys." *Proceedings of the 12th Europ. Conf., Budapest, 1985*, Part I, p. 331.
15. L. SPITZER, *The Physics of Fully Ionized Gases* (Interscience, New York, 1962).
16. R. GRUBER, F. TROYON, D. BERGER, L. C. BERNARD, S. ROUSSET, *et al.*, *Comput. Phys. Commun.* **21**, 323 (1981).
17. L. C. BERNARD, D. DOBROTT, F. J. HELTON, AND R. N. MOORE, *Nucl. Fusion* **20**, 1199 (1980).
18. W. KERNER, P. GAUTHIER, K. LACKNER, W. SCHNEIDER, R. GRUBER AND F. TROYON, *Nucl. Fusion* **21**, 1383 (1981).
19. A. M. M. TODD, J. MANICKAM, M. OKABAYASHI, M. S. CHANCE, R. C. GRIMM, *et al.*, *Nucl. Fusion* **19**, 743 (1979).
20. L. C. BERNARD, F. J. HELTON, R. W. MOORE, AND T. N. TODD, *Nucl. Fusion* **23**, 1475 (1983).
21. L. M. DEGTYAREV, V. V. DROZDOV, A. A. MARTYNOV AND S. YU MADVEDEV, in *Proceedings of the 1984 Int. Conf. on Plasma Phys., Lausanne, Switzerland, 1983*, Vol. 1, p. 157.
22. V. D. SHAFRANOV, *Zh. Tekh. Fiz.* **40**, 241 (1970); *Sov. Phys.-Tech. Phys.* **15**, 175 (1970).
23. D. BERGER, Numerical Computations of the Ideal Magnetohydrodynamic Stability of Small-Aspect-Ratio Tokamaks, Thesis, CRPP-EPF-Lausanne, LRP 131/77, 1977 (unpublished); J. MANICKAM, *Nucl. Fusion* **24**, 595 (1984).
24. A. D. TURNBULL AND F. TROYON, "Contr. Fusion and Plasma Phys.," *Proceedings of the 12th Europ. Conf., Budapest, 1985*, Part III, p. 48; A. D. TURNBULL AND F. TROYON, *Nucl. Fusion*, in preparation.
25. J. P. GOEDBLOED AND P. H. SAKANAKA, *Phys. Fluids* **17**, 908 (1974).
26. H. R. STRAUSS, W. PARK, D. A. MONTICELLO, R. B. WHITE, S. C. JARDIN, M. S. CHANCE, A. M. M. TODD, AND A. H. GLASSER, *Nucl. Fusion* **20**, 638 (1980).
27. G. B. CREW AND J. J. RAMOS, *Phys. Rev. A* **26**, 1149 (1982).